Time- and angle-resolved photoelectron spectrometer based on a picosecond Nd:glass laser system

P. Michelato, L. Monaco, and D. Sertore
INFN Milano-LASA, Segrate, Milano, Italy

I. Pollini[a)]
Dipartimento di Fisica and INFM, Università degli Studi di Milano, Via Celoria 16, 20133 Milano, Italy

(Received 12 September 2002; accepted 14 March 2003)

A time- and angle-resolved photoelectron spectrometer based on an amplified picosecond Nd:glass laser system is described. The kinetic energy of photoemitted electrons, excited by 0.4 ps laser pulses at 264 nm, is measured with a time-of-flight electron energy analyzer. A theoretical model that takes into account the electron drift inside the μ-metal shielded tube as far as the electron analyzer has been introduced to calculate the energy distribution curves of photoelectrons. As a test of the experimental apparatus we present photoemission spectra of cesiated silver excited with 4.7 eV photons. Good agreement between the experimental and the calculated distribution curves of photoemitted electrons has been found. Finally, we have briefly discussed the electronic properties of silver in terms of free electron and *d*-band transitions, together with Auger processes for photon energies near 4 eV. © *2003 American Institute of Physics.* [DOI: 10.1063/1.1574393]

I. INTRODUCTION

Measurements of the ultrafast dynamic behavior of various types of systems in physics, chemistry, and biology have gained much interest during the last decade.[1] The problem of obtaining photoelectron spectra of solids with an energy resolution of the order of some meV or less has also attracted interest in the last years in connection with high-temperature superconductors.[2] One reason for this trend is the availability of laser sources that can produce very short pulses used in time-resolved spectroscopy. Moreover, the interest for high-brillance sources has recently grown due to the development of the free-electron laser (FEL) and related achievements obtained by the Tesla Test Facility (TTF).[3,4] The sources used to generate electron beams in the FEL are mainly radio-frequency guns, where the laser source shines on the photoemissive material and photoelectrons are immediately accelerated to avoid space-charge effects.[5] In this context, a new activity has recently started in the LASA laboratory with the aim of studying the energy distribution curves (EDCS) of electrons emitted from different materials. We have assembled a time-of-flight (TOF) and angle-resolved photoelectron system based on an amplified Nd:glass laser system for measuring the EDC of photoelectron spectra, using 0.4 ps laser pulses at 264 nm. Generally speaking, the use of angle-resolved photoemission spectroscopy (PES) is a powerful and well-established tool for the study of the bulk and surface electronic states of solids. Common sources of radiation for PES are mercury or rare gas lamps, electron-beam-excited x-ray sources, and synchrotron radiation beams, the latter providing a widely tunable short wavelength radiation. Unfortunately, these sources are either continuous or have pulse widths longer than several hundreds of picoseconds and are, therefore, not well suited for time-resolved spectroscopy. Recent advances in nonlinear optics and picosecond-laser technology provide laser-based ultraviolet radiation sources capable of producing ultrashort pulses at a large selection of photon energies up to 25–35 eV.[6]

In order to check the performance of our photoelectron spectrometer, we have measured EDC spectra of silver and cesiated silver. A theoretical model has been also introduced for describing the propagation of the electrons in the materials under investigation and their drift in the tube of the spectrometer. Comparison with low-energy ultraviolet photoemission data reported, for instance, by Berglund and Spicer[7] has shown a fine agreement with our photoemission spectra obtained by time-resolved spectroscopy. To our knowledge, there are only a few papers where a TOF analyzer has been used to study the electronic properties of solids.[8,9] In particular, TOF analyzers have been used for time-resolved spectroscopy of excited states in semiconductors.[10]

In the following sections, we will describe the experimental setup and the operational principle of the TOF spectrometer. We shall also present new photoemission spectra of cesiated silver and discuss the electronic properties of this material at low photon energies where data are scarce.

II. EXPERIMENTAL SETUP

A. Laser system

The radiation source is a solid state laser Twinkle, produced by Light Conversion, LT, based on Nd:glass. It operates at 12.5 Hz producing IR light (1055 nm) with an energy of 1.5 mJ. A passive mode-locked (dye cell) master oscillator with negative feedback (for stable seeding pulse generation) produces 1.2 ps pulses that, after a grating stretching unit, seeds a regenerative amplifier (RA). At the RA exit, after a

[a)]Author to whom correspondence should be addressed; electronic mail: iempollini@mi.infm.it

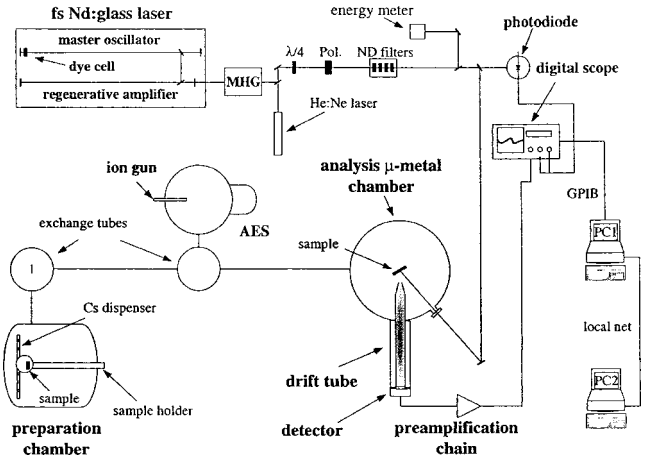

FIG. 1. Schematic layout of the time-of-flight spectrometer, including the preparation chamber, the AES apparatus, the laser, and the PC-based acquisition system.

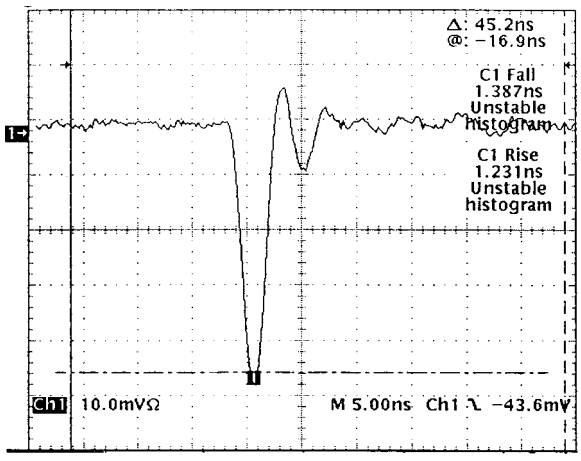

FIG. 2. Typical oscilloscope signal observed after the preamplifier chain. Rise time is less than 2 ns.

grating compression unit, the IR pulse length is approximately 1.2 ps. The IR pulse then passes through a special second harmonic generator and optical compression unit (type II),[11] at whose exit the pulse wavelength is 527 nm and the pulse length is approximately 0.4 ps. The UV pulse ($\lambda = 264$ nm), generated using a KDP crystal, has a similar time structure. The fifth harmonic ($\lambda = 211$ nm) is generated combining the first and fourth harmonics on a BBO crystal.[12] Both the IR and green pulse lengths can be monitored using a single shot autocorrelator, while the fourth-harmonic pulse is monitored using both a spectrometer and a conventional delay line autocorrelator based on a self-diffraction technique on a thin quartz plate.[13] The laser pulse incident on the cathode is monitored by a fast photodiode, whose signal is then used as a trigger signal sent to the digital oscilloscope (Tektronix TDS 684C), used for the data acquisition.

B. Time-of-flight spectrometer

The principle of a TOF spectrometer is simple. By measuring the time T in which an electron flies through a distance L, we know the kinetic energy of electrons E_k. It turns out that in order to get a high-resolution TOF spectrometer, it is necessary to let the electrons fly for a long distance and measure the flight time precisely. The experimental apparatus consists primarily of an ultra-high-vacuum (UHV) chamber and the Nd:glass laser system previously described. The main parts of the UHV system are a cathode preparation chamber (base pressure $\sim 10^{-10}$ mbar), where samples are cesiated, an Auger electron spectroscopy (AES) analyzer equipped with an ion gun for sample cleaning, and a chamber for PES studies, where the low-energy TOF analyzer is installed (base pressure $\sim 10^{-10}$ mbar) (see Fig. 1). The AES spectrometer is used to check the surface cleaning of samples before making the TOF measurements. The vacuum chamber has six Suprasil 2 viewports for the laser light entrance between 20° and 80°. A turnable sample holder allows us to change the sample-analyzer angle. The TOF spectrometer consists of a 439-mm-long drift tube, where photoelectrons fly along in the presence of the unavoidable residual electric and magnetic fields. A pair of microchannel plates (MCPs), used in chevron configuration, detect the electrons at the end of the drift tube. The gain of the MCP in this configuration is 10^6. The operating voltage across the MCPs is 1850 V with a typical current of 63 μA. The detector output has a 50 Ω impedence to reduce the output-pulse shape distortion and to ensure a nanosecond rise time. Two preamplifiers connected in series amplify the detector signal: a VT110 preamplifier is then connected to the detector output and it is followed by a 9301 (EG&G). The pulse rise time at the end of the preamplifier chain is less than 2 ns, as shown in Fig. 2. The time delay of the preamplifier signal with respect to the start trigger operated by the photodiode gives the electron flight time. All data are then collected by using a PC-based acquisition system: whenever the signal coming from the preamplifier chain is above the threshold level, the acquisition system counts a collected electron.

C. Energy analyzer

The TOF detector consists of an analysis μ-metal UHV chamber, a drift tube, and the readout electronics. An UHV transfer system allows the photocathode samples to be moved from the preparation chamber to the TOF analyzer. A high-precision longitudinal and rotational translator allows us to position the samples in front of the detector and to change the angle between the sample and analyzer. The electron kinetic energy is given by

$$E_k = 1/2m(L/T)^2, \tag{1}$$

where T is the electron time of flight, L the drift length, and m the electron mass.

Many effects can affect the energy and distribution of collected electrons; among the most important are the space charge field and the residual electric and magnetic fields. The space charge field is due to the mutual interaction of electrons in the flying bunch from the cathode to the detector. Many papers have been devoted to this phenomenon[14–16] and this work showed that key elements are the charge emitted per pulse and the current density. In the case of photoemission measurements using short pulses, even a low charge density can lead to a high current density. However, in our experiment the laser spot size on the sample has a radius of

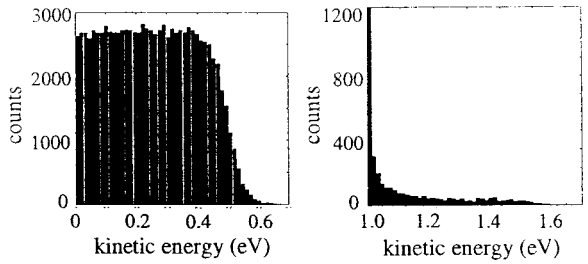

FIG. 3. Effect of the electric field on a Fermi distribution. Electrons are generated with a Fermi energy of 0.5 eV and drift under the influence of a potential difference of 1 V applied between the sample and the spectrometer nose.

about 1.4 mm and the total number of emitted electrons is less than a few thousands per shot, and so, by taking into account the laser pulse duration of 0.5 ps, the current density is about 50 mA/cm^2. In this condition, the effect of the space charge can be neglected,[14,17] as a first approximation.

The effect of the residual electric field inside the flight tube can also change the electron energy as well as the number of collected electrons. The first aspect is due to the presence of the field that, depending on the sign of the potential, can accelerate or decelerate the photoemitted electrons, while the second one is caused by an electrostatic lens effect related to the analyzer geometry. Sources of residual electric fields are the contact potentials between the sample and surrounding components and the building up of a charge due to dielectric layers. In our case, the contact potentials have been balanced by applying a proper voltage between the sample and the spectrometer, while the charging up is prevented by gold plating the flight tube components.

The residual magnetic field can further affect the electron trajectory and, therefore, the number of collected electrons. In order to minimize its effect, all hardware components around the spectrometer are built up with a μ-metal to shield out stray magnetic fields. Exceptions to this are the 316LN CF flanges, necessary to make the connection between the spectrometer and the analysis chamber. To avoid a magnetic field flow inside the chamber through the flanges, an external shield, designed and optimized using the POISSON code,[18] has been installed on the system so as to reduce the magnetic field along the drift tube axis to 25 mG.

Even if we have reduced the strength of the residual electric and magnetic field, their effect can still be quite important. For these reasons, we have evaluated their influence on the EDC spectra by developing a model that takes into account the effect of both fields. Since, under our experimental conditions, the space charge effect should be negligible, in our simulation model we have neglected the electron mutual influence. As expected from the spectrometer geometry, the effect of the residual electric field is to accelerate electrons mainly along the TOF axis, if there is a negative potential between the sample and the analyzer nose. This effect raises the electron energy and allows more electrons to enter the TOF collection cone, since it increases the velocity component along the TOF axis. As a consequence, the photoemission spectrum is shifted and distorted at low energies because of a larger number of collected electrons. In Fig. 3 we have shown the result of one simulation, where we have

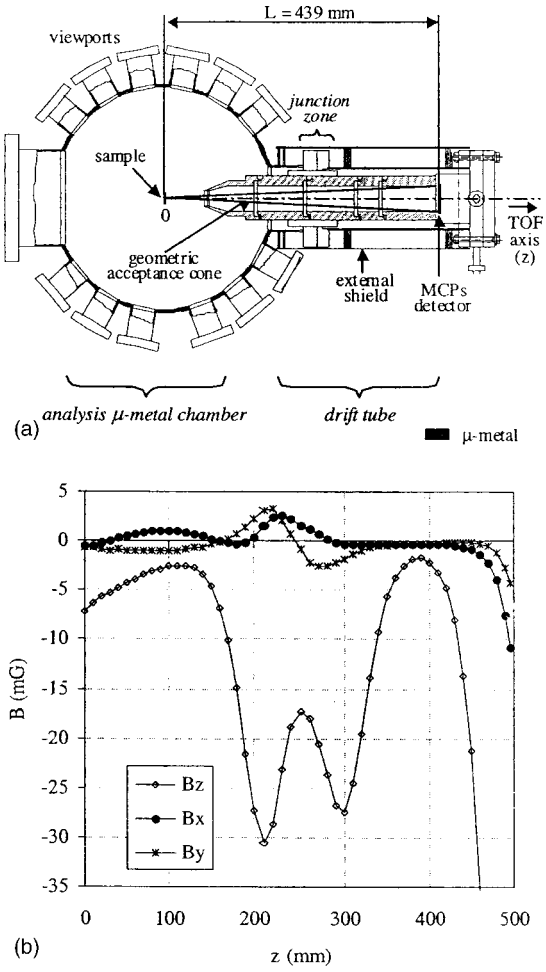

FIG. 4. (a) Sketch of the analysis chamber and drift tube for TOF measurements. The picture shows the sample position ($z=0$ mm), the flight distance L, and the viewports for the entrance of the laser radiation. (b) Residual magnetic field components measured along the drift tube axis (sample position at $z=0$ mm; detector position at $z=439$ mm). Note the strong variation of the longitudinal component (also, the position of the two maxima) in the shielded junction zone (between the chamber and the drift tube), where the 316LN CF flanges are used.

studied the distortion on a Fermi distribution with Fermi energy $E_F=0.5$ eV, due to an accelerating potential of 1 V.

The three spatial components of the residual magnetic field (see Fig. 4), measured along the TOF tube axis with a flux-gate magnetometer, have been also included in the simulation program. The main effect of the magnetic field is to modify the electron trajectories, which is important for emission angle measurements. In Fig. 5(a), we have shown the distortion of electron trajectories caused by the residual magnetic field, as obtained by our simulation program. Our procedure was to generate monoenergetic electrons, with low kinetic energy ($E_k=0.2$ eV) and directed inside the geometry of the collection cone, and then to start the simulation program. The magnetic field can prevent low-energy electrons from reaching the MCP detector. This effect is evident in our PES measurements. For example, in Fig. 5(b), the Fermi distributions ($E_F=0.5$ eV), measured before and after the electron flight towards the detector, are compared and one can see how the resulting spectrum is mainly affected at low kinetic energy. This simulation result has been obtained

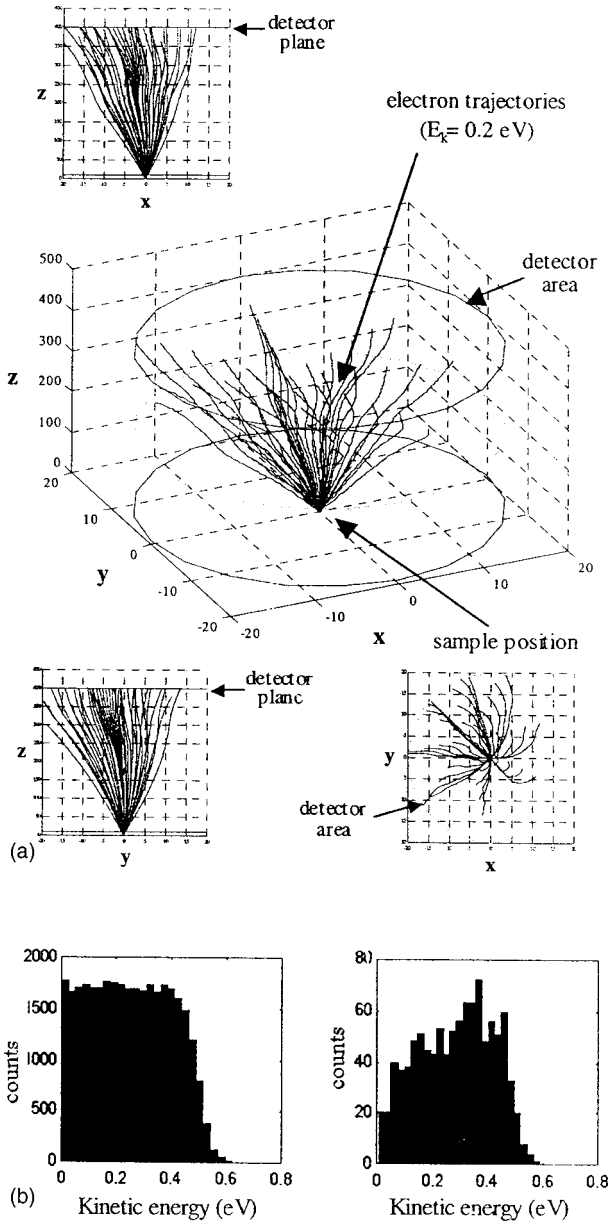

FIG. 5. (a) Simulation of the residual magnetic field effect on the electron paths inside the drift tube for monoenergetic electrons ($E_k = 0.2$ eV). Projections along the Cartesian axes are also reported. (b) Influence of the residual magnetic field on the Fermi distribution. The simulation obtained for a distribution with a Fermi energy of 0.5 eV shows a cut in the electron counting at low kinetic energy (from 0 to 0.2 eV). The figure also shows a comparison between the electron energy distributions before and after the flight in the TOF tube.

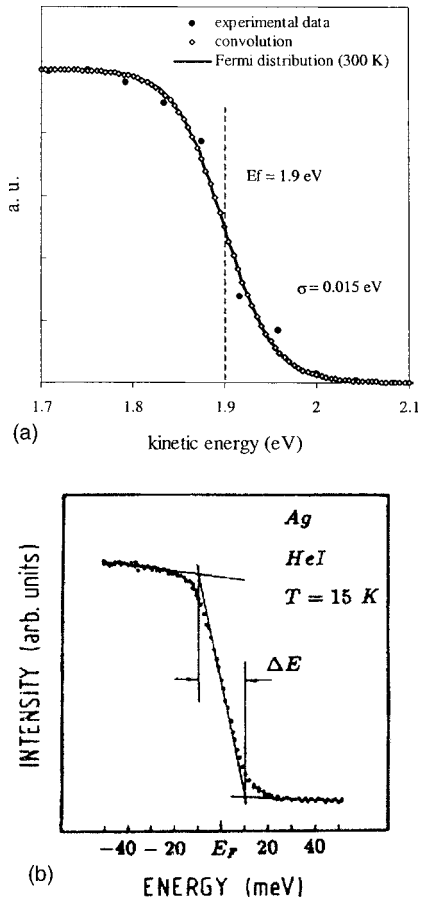

FIG. 6. (a) Energy resolution of our TOF spectrometer measured on a cesiated silver sample: the resolution is $\sigma = 0.015$ eV for the Fermi energy of 1.9 eV. (b) High-resolution photoelectron spectra from a silver metal around the Fermi energy and its analysis in terms of the Fermi function and Gaussian broadening (adapted from Ref. 19).

by considering the value of the residual magnetic field measured inside the TOF tube and the geometrical dimension of our spectrometer.

The spectrometer energy resolution is given by

$$\Delta E/E = 2\sqrt{(\Delta T/T)^2 + (\Delta L/L)^2}, \tag{2}$$

where $T(E)$ is the transit time, L is the transit distance, ΔT is the uncertainty in the transit time, and ΔL is the uncertainty of the transit distance. We have determined the energy resolution of our spectrometer by measuring many photoemission spectra from cesiated silver samples and comparing their Fermi edge with the convolution of the Gaussian distribution with the Fermi function at 300 K. The standard deviation of the distribution gives the energy resolution of the spectrometer. Figure 6(a) shows an example of our measurements made at kinetic energy of 1.9 eV. The 15 meV energy resolution we have obtained is in excellent agreement with the theoretical value of 14 meV calculated with Eq. (2), under the assumption that the major contribution will be given by the 2 ns uncertainty due to the acquisition system. It is worth comparing our result with those obtained in PES. In good PES instruments the spectrometer resolution is of the order of 10 meV and, therefore, it allows, for example, a very detailed study of temperature effects or the investigation of excitation spectra of solids close to the Fermi energy. An example of a high-resolution photoemission spectrum from silver around the Fermi energy, together with its analysis in terms of the Fermi function and Gaussian broadening, has been made at 15 K by Patthey *et al.*[19] with photon excitation of 21.2 eV. The energy resolution of this PE spectrometer was found around 25 meV in line with our results in Fig. 6(b). At lower energy, however, the energy resolution of a TOF spectrometer may worsen somewhat, due to the effect of the residual magnetic field. In our case, we have measured an energy resolution close to 25 meV at 0.4 eV.

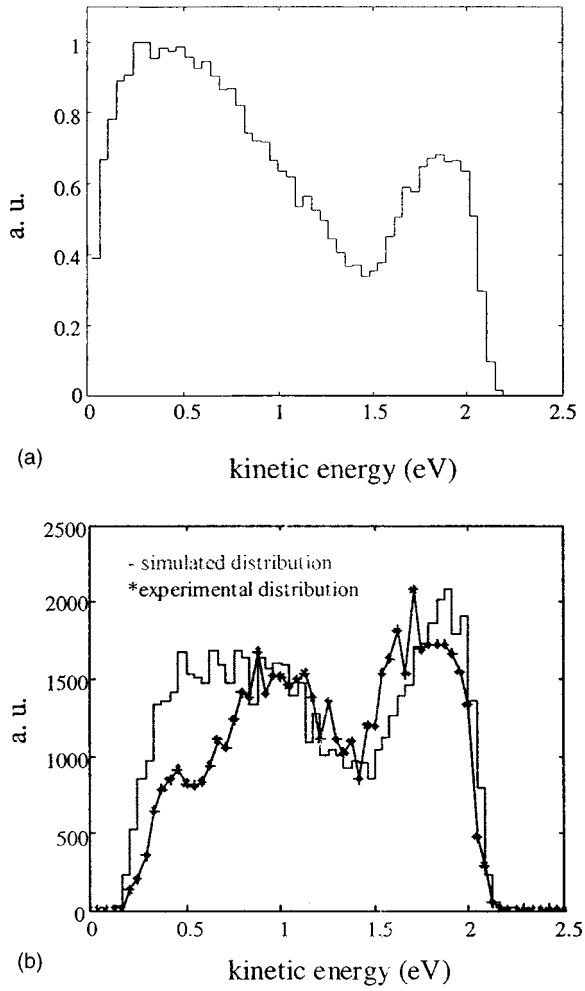

FIG. 7. (a) Calculated electron EDC at the sample surface. (b) Comparison of the experimental EDCs of photoelectrons after their drift in the TOF tube with the simulated electron EDC.

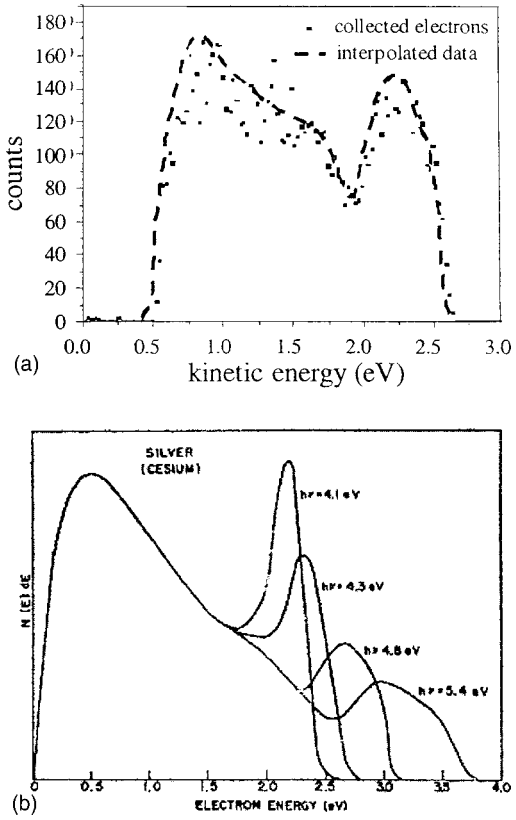

FIG. 8. (a) Cesiated silver spectrum obtained with the TOF technique, using exciting photons of 4.7 eV. (b) EDC spectra of photoelectrons from cesiated silver excited at photon energy $h\nu = 4.3$, 4.5, and 5.4 eV (adapted from Ref. 7).

III. PERFORMANCE

In order to test our spectrometer we have chosen a well-known material like cesiated silver. The electronic structure of silver and cesiated silver had been studied in photoemission a long time ago.[7,20] The cesiation process covers the silver surface with 1 ML (or less) of cesium, and reduces the Fermi edge from 4.25 to 2.9 eV, so that it is possible to probe deeper levels in the conduction band of silver.[7,21]

Figure 7(b) shows the experimental EDC spectrum of cesiated silver for photon energy at 4.7 eV, measured after balancing the contact potential. This spectrum has been then compared with the electron energy distribution curve determined by considering the theoretical joint density of states of silver.[22] The calculated EDC spectrum takes into account both the electron propagation in the sample, including electron–electron scattering and Auger processes [Fig. 7(a)], and the electron flight in the drift tube under the influence of the residual magnetic and electric fields [Fig. 7(b)]. The good agreement above 0.5 eV between the experimental and the theoretical distribution curves confirms the validity of our model. At low energy, where the magnetic residual field can strongly perturb the electron distributions, we believe that the difference between the experimental and calculated spectra is mainly due to the approximation of cylindrical symmetry assumed for the expansion of the magnetic and electric fields out of the axis in the calculation. In fact, the measurements of the residual magnetic field have been done only along the TOF axis, due to the sensitive volume of our probes with respect to the dimension of the drift tube.

Moreover, the fine agreement between the TOF spectra with the low-energy ultraviolet photoemission spectra reported in the literature[7] confirms the validity of our procedure and analysis and gives further new insight into the electronic properties of cesiated silver at these photon energies. In this spirit, we have shown in Fig. 8(b) the experimental electron EDC spectra for photon energies at 4.1, 4.3, and 5.4 eV, reported by Berglund and Spicer,[7] together with our electron EDC spectrum excited with 4.7 eV photons [Fig. 8(a)]. Our spectrum has been accelerated by a few hundreds of meV in order to measure also the low kinetic energy electrons, which would not have been collected otherwise because of the influence of the residual magnetic field. First of all, we can note that our spectrum is very similar and consistent with those measured by ultraviolet photoelectron spectroscopy. Then, we see that, except for the high-energy peak (observed for E_k between 1.7 and 2.7 eV in Fig. 8) associated with a peak in the density of states at 0.3 eV below the Fermi level, the electron EDC spectra are well described by the energy distribution curves due to the Auger process and electron–electron scattering.[7] As for the high-energy peak, Erenreich and Philipp[23] have shown in detail

that interband transitions do not become dominant in silver until the photon energy $h\nu > 3.5$ eV and that only a "free-electron" absorption can be active for energies $h\nu < 3.5$ eV. The energy distribution curves of photoemitted electrons for $h\nu < 3.5$ eV shown by Berglund and Spicer illustrate this point very well. The peak at $E_k = 2.25$ eV, near the maximum electron energy, becomes more apparent as the photon energy increases, but does not dominate the distribution. This peak is due to direct transitions from the peak in the density of states at the critical point L_2', as shown, for instance, in the electronic band structure calculated by Segall.[24] It also turns out that the low-energy peak at $E_k = 0.75$ eV, due mainly to Auger processes, begins to appear when the photon energy is approximately 4 eV and that at higher photon energies the EDCs are essentially independent from the photon energy.[7] The characteristic electron distributions due to the Auger effect should also be relatively constant in shape and magnitude for excitations around 4.0–4.2 eV, until *d* electrons are excited directly in the energy distributions at about 5.7–5.8 eV, obscuring the Auger distribution curves.

IV. DISCUSSION

We have assembled a time-of-flight and angle-resolved photoelectron system based on an amplified Nd:glass laser system for measuring the EDC of photoelectron spectra using 0.4 ps laser pulses at 264 nm. We have then discussed the possibility of obtaining photoelectron spectra near the Fermi level with an energy resolution of 15 meV by means of a TOF analyzer and an UV laser light source. The TOF technique is particularly useful for laser photoemission since the light source is pulsed and the detector is not restricted to a particular energy window. The photoemitted electrons drift for a 439 mm distance through a μ-metal shielded tube before reaching the electron detector. The detector consists of a grounded stainless mesh, a pair of chevron microchannel plates, and a single detection anode with stop electronics. The apparatus allows us to measure the energy distribution curves of photoelectrons emitted with kinetic energy between 0 and 5 eV. As a test of the experimental system, we have examined the electron energy distribution curves from cesiated silver samples excited with 4.7 eV photons and have briefly discussed the silver electronic properties in terms of free-electron and *d*-band transitions, together with electron–electron scattering and Auger processes, which are active for photon energies near 4 eV. We have also developed a simulation model for describing the transport of electrons both in the examined materials and in the drift tube of the spectrometer, by taking into account the residual magnetic field, which produces a cut in the photoemission spectrum below 0.25 eV, as observed in our photoemission spectra.

ACKNOWLEDGMENT

Partial financial support by the FIRST institution for the present research is acknowledged by the authors.

[1] *Ultrafast Phenomena IX*, edited by P. F. Barbara, W. H. Knox, G. A. Morou, and A. H. Zewail, Vol. 60, Springer Series in Chemical Physics (Springer, Berlin, 1994).
[2] G. Margaritondo, D. L. Huber, and C. G. Olson, Science (Washington, DC, U.S.) **246**, 770 (1989).
[3] J. Andruskov *et al.*, Phys. Rev. Lett. **85**, 18 (2000).
[4] V. Ayvazyan *et al.*, Phys. Rev. Lett. **88**, 104802 (2002).
[5] J. S. Fraser and R. L. Sheffield, IEEE J. Quantum Electron. **QE-23**, 1489 (1987).
[6] J. Boker, P. H. Buckssbaum, and R. R. Freeman, Opt. Lett. **8**, 21 (1983).
[7] C. N. Berglund and W. E. Spicer, Phys. Rev. **136**, A1030 (1964).
[8] R. Z. Bachrach, F. C. Brown, and S. B. M. Hagstrom, J. Vac. Sci. Technol. **12**, 309 (1975).
[9] G. Paolicelli *et al.*, Surf. Rev. Lett. **9**, 541 (2002).
[10] R. Haight and J. A. Silberman, IEEE J. Quantum Electron. **QE-25**, 2550 (1989).
[11] A. Umbrasas, J. Diels, J. Jacob, G. G. Valiulis, and A. Piskarsas, Opt. Lett. **20**, 2228 (1995).
[12] A. Dubietis, G. Tamosauskas, A. Varanacius, G. Valiutis, and R. Danielius, Opt. Lett. **25**, 1116 (2000).
[13] H. J. Eichler, P. Guenter, and D. W. Pohl, *Laser Induced Dynamics Gratings* (Springer, Berlin, 1986).
[14] T. Gilton, J. P. Cowin, G. D. Kubiak, and A. V. Hamza, J. Appl. Phys. **68**, 4802 (1990).
[15] M. V. Ammosov, J. Opt. Soc. Am. B **8**, 2260 (1991).
[16] A. S. Aleksandrovsky and V. V. Slabko, J. Electron Spectrosc. Relat. Phenom. **74**, 149 (1995).
[17] J. Bokor *et al.*, Phys. Rev. B **32**, 3669 (1985).
[18] J. H. Billen, Documentation, Los Alamos, National Laboratory, August (1996).
[19] F. Patthey, J. M. Imer, W. D. Schneider, Y. Baer, and B. Delley, Phys. Rev. B **42**, 8864 (1990).
[20] N. V. Smith, Phys. Rev. B **3**, 1862 (1971).
[21] P. Michelato *et al.*, EPAC 2000 Wien, June (2000).
[22] Dr. Papaconstantopoluos database: http://cst-ww.nrl.navy.mil/esdata/database.html(EDJDOS).
[23] H. Ehrenrech and H. R. Philipp, Phys. Rev. **128**, 1622 (1962).
[24] B. Segall, Phys. Rev. **125**, 109 (1961).